PCCP

Accepted Manuscript

ROYAL SOCIETY OF CHEMISTRY

www.rsc.org/pccp

Cite this: DOI: 10.1039/c0xx00000x

www.rsc.org/xxxxxx

ARTICLE TYPE

Charge transport in films of *Geobacter sulfurreducens* on graphite electrodes as a function of film thickness

Partha Sarathi Jana,[a] Krishna Katuri,[a,b] Paul Kavanagh,[a] Amit Kumar[a,c] and Dónal Leech*[a]

Received (in XXX, XXX) Xth XXXXXXXXX20XX, Accepted Xth XXXXXXXXX 20XX
DOI: 10.1039/b000000x

Harnessing, and understanding the mechanisms of growth and activity of, biofilms of electroactive bacteria (EAB) on solid electrodes is of increasing interest, for application to microbial fuel and electrolysis cells. Microbial electrochemical cell technology can be used to generate electricity, or higher value chemicals, from organic waste. The capability of biofilms of electroactive bacteria to transfer electrons to solid anodes is a key feature of this emerging technology, yet the electron transfer mechanism is not fully characterized as yet. Acetate oxidation current generated from biofilms of an EAB, *Geobacter sulfurreducens,* on graphite electrodes as a function of time does not correlate with film thickness. Values of film thickness, and the number and local concentration of electrically connected redox sites within *Geobactor sulfurreducens* biofilms as well as a charge transport diffusion co-efficient for the biofilm can be estimated from non-turnover voltammetry. The thicker biofilms, of 50 ± 9 µm, display higher charge transport diffusion co-efficient than that in thinner films, as increased film porosity of these films improves ion transport, required to maintain electro-neutrality upon electrolysis.

Introduction

Microbial fuel cell (MFC) devices that use EAB to oxidize organic substrates, degrading wastes and generating electricity, have received a great deal of attention in recent years.[1-4] Proposed mechanisms of electron transfer within films of EAB to produce current at solid anode surfaces include, production and use of electron shuttling mediating molecules[5] and redox active membrane-bound proteins (cytochromes),[6, 7] self-exchange within redox conducting films[7, 8] or even, controversially, *via* conductive nanowires (pili).[9] The exact mechanism or combination of mechanisms that drive electron transfer within films of EAB to solid surfaces is not yet, however, fully understood. Studies on biofilms of *Geobacter sulfurreducens* (GS) on electrodes for acetate oxidation, as a model EAB, have provided information on electrical communication between EAB and anodes.[10-14] In recent years use of electroanalytical,[14-17]and spectroelectrochemical[7, 18, 19] techniques, often in combination with genetic engineering,[6] immunohistochemical staining,[20] or NMR[21] has helped elucidate the role of electron transferring species (cytochromes, pili) in current production by GS biofilms on anodes. For example, genomic analysis of GS has identified coding sequences for periplasmic cytochromes, membrane cytochromes and other outer membrane proteins that can contribute to extracellular electron transport.[8, 13, 22-26] Recently, three electrode electrochemical cell configurations were used to induce biofilm growth on anodes, under a controlled applied potential versus a reference electrode, to achieve better control of the anode potential during biofilm growth, over use of a fixed resistance load imposed between anode and cathode.[14,23, 25] However, how cells and cellular components coordinate in the transport of electrons through a thick biofilm and across the biofilm anode interface and what limits the rate and distance that electrons can be transported through an EAB biofilm remains unresolved.[27] Little has yet been reported on how film thickness can affect how, and how rapid, charge is transported through GS biofilms on solid electrodes, and how this contributes to catalytic acetate oxidation current generation. Marsili *et al.*[22] reported on the correlation between the mass of protein from GS developed on electrodes as a function of time, and they observe an increment in acetate oxidation, from 2 mA mg^{-1} protein initially to 8 mA mg^{-1} protein within 6 hours of bacterial growth. Most recently Bond *et al.*[27] proposed that biofilms will grow in thickness until either the pH value near the anode surface becomes sufficiently low to inhibit cytochrome function of the innermost cells, thereby limiting the ability of all cells in the biofilm to transfer electrons to the anode, or until the local concentration of oxidized cytochromes experienced by the outermost cells becomes too low to support additional growth. Here we report on GS biofilm production on graphite rod electrodes under continuous mode operation, using a multi-channel potentiostat to control the potential applied to multiple electrodes, permitting temporal sampling of biofilms under controlled conditions. This allows for a comparison of biofilm thickness over time to voltammetric responses in the presence and absence of acetate as electron donor. In the absence of electron donor, redox site concentration, within the biofilms, and charge transport across the biofilm vary as a function of film thickness, providing an insight into the factors that may affect current generation on microbial fuel cell anodes.

Materials and methods

Experimental set-up

The study was carried out in a single-chambered electrochemical cell of 800 mL volume with multiple working electrodes assembled concentrically placed around a single counter and reference electrode (Fig. 1). Eight graphite rods (3 mm diameter, Graphite Store product NC001300) with exposed area of 1.77 cm^2 each were used as working electrodes. Platinum mesh (2.5 cm × 2.5 cm dimension, Sigma-Aldrich, Dublin) was used as counter electrode and custom built Ag/AgCl (3 M KCl) with a porous vycor frit (Advanced Glass and Ceramics) acting as salt bridge were used as reference electrode. In this configuration influent was supplied to the cell from the bottom of the chamber using a peristaltic pump (Gilson, France) with effluent exiting the chamber at the top of the reactor, as shown in Figure 1.

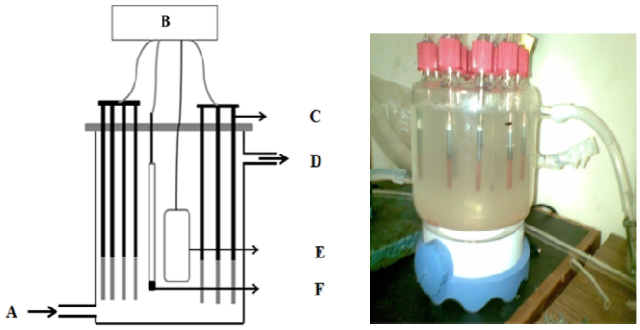

Fig. 1 Schematic diagram left, and photograph, right, of the anaerobic electrochemical cell, where (A) is feed inlet (B) potentiostat (C) working electrodes with dark grey colour in diagram representing the available surface area, and the pink/red colour in the photograph indicative of GS biofilm formation, (D) is outlet (E) counter electrode and (F) reference electrode.

Biofilm growth on electrode surface

Geobacter sulfurreducens (ATCC 51573) was used as a source of electroactive bacteria. The strain was sub-cultured in 100 mL airtight, rubber septa-sealed, anaerobic syringe bottles containing 90 mL of growth medium, prepared according to the protocol supplied by the culture centre (http://www.dsmz.de, medium no. 826). The bacteria were cultured in fumarate-containing *Geobacter* growth medium for 2 weeks (three sub-cultures) prior to inoculation in the electrochemical cell. Following inoculation biofilms were induced to grow on graphite-rod electrodes, with eight electrodes in the same electrochemical cell, under a constant applied potential (0 V vs Ag/AgCl) using a multichannel potentiostat (CHI-1030a, CH Instruments, Austin, TX). Growth media containing acetate as a source of electron donor (10 mM) was used as feed. The feed pH was in the range of 7.2-7.5 throughout the experiment and the cell was operated at temperatures that varied from 28 to 32 °C. Initially the reactor was operated over a single batch feed, by inoculation with GS directly from the culture bottles in an anaerobic glove-box, and operation under 0 V applied potential for 65 hours to encourage the attachment of bacteria to the graphite rod working electrodes. Thereafter the electrochemical cell was operated using continuous delivery of anaerobic, nitrogen-sparged, acetate-containing medium only (no further inoculum) with a peristaltic pump using a flow rate of 8.3 mL h^{-1}, with additional mixing within reactor provided by magnetic stirring at a rate of 50 rpm.

Cyclic Voltammetry

Stirring, and flow of media, was halted for 30 minutes prior to recording of *in-situ* cyclic voltammetry (CV) in the reactor. Non-turnover CV was recorded after removal of acetate from the electrode-attached biofilms, by washing electrodes, sampled under anaerobic conditions from the reactor, in acetate-free culture medium. The electrodes were then transferred into a separate vessel containing 100 mL of acetate-free culture medium and incubated for 30 min under anaerobic conditions to ensure dilution of the acetate concentration in the biofilm matrix. The electrodes were subsequently transferred into a separate electrochemical cell containing 100 mL of acetate-free culture medium to perform non-turnover CV.

Confocal laser scanning, and electron, microscopy

Electrodes removed from the reactor were sectioned into two pieces for subsequent scanning electron microscopy (SEM) and confocal laser scanning microscopy (CLSM) imaging. Prior to SEM imaging, fixation was undertaken, using a series of primary and secondary fixatives,[28, 29] by placing the electrode in the following solutions: (a) 1% glutaraldehyde, 2% paraformaldehyde, 0.2% picric acid, 10 mM 2-[4- (2-hydroxyethyl)-1-piperazinyl]ethanesulfonic acid (HEPES, pH 7.4) for 1 h, (b) 50 mM NaN_3 for 1 h, (c) 2% tannic acid for 1 h, (d) 1% osmium tetroxide for 2 h, (e) 1% thiocarbohydrazide for 30 min, and (f) 1% osmium tetroxide overnight, with washing using 10 mM HEPES buffer (pH 7.4) between steps (all Sigma-Aldrich). The samples were then dehydrated in a graded series of aqueous ethanol solutions (10-100%) and oven-dried (2 h at 40 °C) to remove residual moisture. The dried samples were mounted over SEM stubs with double-sided conductivity tape and a thin layer of gold metal applied using an automated sputter coater (Emitech, K550) for 2 min and imaged using a model 4700 SEM instrument (Hitachi, Japan). For CLSM imaging, electrode sections were transferred into sterile vessels containing 50 mL of anaerobic acetate-free growth medium. The graphite rod was cross-sectioned into pieces (~3 mm in height) using a scalpel and stained, by incubation for 15 min in 10 mL of 10 mM potassium phosphate buffer, pH 7.0, containing 1 µL of propidium iodide and 1µL of syto 9 from a Molecular Probes bacLight LIVE/ DEAD L7012 stain kit (Invitrogen Corp., Carlsbad, CA) in the dark. The samples were then gently washed in phosphate buffer (10 mM, pH 7.0) to remove unbound residual dye from the biofilm matrix. The sectioned face of the rod was placed on a multi-well microscope slide to examine horizontal growth of biofilm through a Zeiss LSM 510 axiovert inverted confocal microscope with a 40× achroplan oil immersion lens. A minimum of 10 fields of biofilm views were imaged, and Z-series images were processed and analysed with Zeiss LSM510 operating software for biofilm thickness measurements (supplementary information). Images were obtained using an excitation wavelength of 488 nm and a BP500−550 emission filter for green fluorescence. The excitation wavelength was 543 nm, and emission filter LP605 was used to obtain images for red fluorescence.

Results and discussion

The three electrode electrochemical cell configuration using acetate as an electron donor, no deliberately adding electron acceptor, and a potential of 0 V vs. Ag/AgCl applied to the working electrodes initiates GS respiration on the polarised working electrodes, and subsequent biofilm growth. Eight graphite electrodes were used as working electrodes in the same electrochemical cell, allowing each electrode to experience similar conditions (temperature, feed, ionic strength, pH etc) and permitting removal of pairs of electrodes at intervals during the biofilm growth period.

A disadvantage of using a single chamber electrochemical cell is that the counter electrode reaction products are free to diffuse to the working electrode and this could potentially generate uncontrolled experimental parameters.[30, 31] For example, in a single chamber three electrode cell, diffusion of hydrogen produced at the counter electrode to the working electrode can be utilized by EAB to produce a current higher than that expected with the supplied electron donor.[24, 32] In use of non-separated anode and cathode, in three electrode electrochemical cells can result in different trends in the anode potential required for maximum steady-state current density from biofilms induced to grow on electrodes using mixed-culture innocula.[31, 33] Continuous flow reactors operation is thus used to remove electrolysis products whilst ensuring that substrate (fuel) is available for current production, simplifying analysis of results. The applied potential of 0 V vs Ag/AgCl was chosen based on CV analysis[14, 34] to provide sufficient driving force to drive electron transfer from biofilm to solid electrode surface.[11, 23, 35, 36]

After inoculation, an increase in the oxidation current production was observed over time, Figure 2. Although the amperometric trace is the sum of the current through all interconnected graphite working electrodes, it was confirmed that each individual electrode responds in a similar, reproducible, manner, by connecting each as a working electrode in a slow-scan CV experiment at defined intervals along the growth curve, Figure 3A. For example, the CV response sampled for each electrode produces steady-state acetate oxidation current densities (*vide infra*) of 4.0 ± 0.4 A m^{-2} after 65 h, 5.8 ± 0.4 A m^{-2} after 79 h and 7.0 ± 0.3 A m^{-2} after 129 h operation in the reactor.

The pattern of biofilm growth and current generation can vary depending on a range of factors, such as feed concentration, inoculum concentration and stage, electrode material, and potential.[2, 3, 14] In this study we observe a 45 h lag phase prior to commencement of a rapid increase in current production, associated with the exponential growth phase for the bacterial biofilm. Others have reported a similar trend to current production by electrode-attached GS biofilms on graphite in electrochemical reactors. For example, Fricke *et al.*[17] and Torres *et al*.[37] report current generation within 100 hours of reactor start-up for biofilms of GS on carbon electrodes using acetate as model substrate. Slight differences in the lag phase duration may be due to differences in the selected anode potential or electrochemical cell configuration to induce biofilm current generation.

After 65 h of operation in 10 mM acetate as electron donor in *Geobactor* medium, without any added electron acceptor, the electrochemical cell was switched to continuous mode at a flow rate of 200 ml/day to prevent electron donor depletion and to wash out suspended bacteria. The rapid growth in current at this stage indicates that GS electroactive bacteria are capable of transferring electrons to the anode as a result of acetate oxidation, with SEM, CLSM and cell count results (*vide infra*) demonstrating formation of layers of GS cells on the electrode surface.

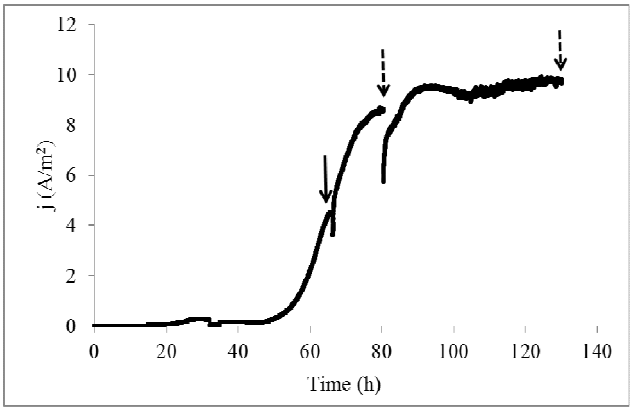

Fig. 2: Amperometric response of graphite rod working electrodes, as a function of time, during GS biofilm growth operation (10 mM acetate) under 0 V vs. Ag/AgCl applied potential. Solid arrow indicates the region where the reactor was switched from batch to continuous mode operation. Arrows represent biofilm sampling points for analysis by *in-situ* CV, *ex-situ* CV, and for biofilm thickness.

Current generation increases from 45 to 85 h until a steady state current of ~9 A m^{-2} is reached, providing current densities similar to those reported on previously. For example, Marsilli *et al.*[22] reported a steady-state current density, in 20 mM acetate, of 4-7 A m^{-2} achieved after 72 hours under an applied potential of 0.04 V vs. Ag/AgCl by GS biofilms at graphite or roughened glassy carbon electrodes. More recently, Katuri *et al.*[14] reported a steady-state amperometric current density for actetate oxidation by GS biofilm on carbon electrodes of 9.2 A m^{-2} after 142 h of repeated batch mode experiments.

A series of experiments was conducted at defined times during the operation of the reactor to examine the correlation between current generation, content of redox active material, and biofilm thickness. This was possible as all 8 electrodes showed similar current generation capabilities (Fig 3A) permitting sampling of electrodes from the reactor at defined times, as follows. The *in situ* voltammetric behaviour of biofilms was recorded at the time intervals of 65, 79 and 129 h after reactor initiation, using slow-scan cyclic voltammetry. Redox-active content of biofilms was probed using *ex-situ* voltammetry of one sampled electrode, at each of these times, recorded in growth medium with no added substrate (acetate), whilst *ex-situ* microscopy (SEM/CLSM) and fluorescence microscopy of biofilms on a second sampled electrode at each of these times was used to provide information on film thickness.

Sigmoidal shaped cyclic voltammograms recorded at the time intervals of 65, 79 and 129 h after reactor initiation, using slow-scan cyclic voltammetry, permit estimation, from the first derivative of the voltammogram, of acetate oxidation centered at −0.41 V vs. Ag/AgCl in good agreement with that reported on by others.[7, 13, 17, 34, 37, 38] The sigmoidal shaped voltammogram, with examples shown in Fig. 3, is indicative of catalytic oxidation of the acetate substrate by the biofilm with heterogeneous electron

transfer to the electrode, with similar responses reported on for acetate oxidation by biofilms of GS.[34]

The change in magnitude of the steady-state catalytic oxidation current observed in the slow scan cyclic voltammograms as a function of time and growth conditions correlate with the changes observed in amperometric current over the same period. It is to be noted however that amperometric currents are higher than the steady-state catalytic currents observed in the slow-scan cyclic voltammograms. Convective substrate mass transport may provide an additional contribution to current in the reactor during amperometry compared to that during *in-situ* voltammetry, as the flow of media was stopped 30 minutes prior to recording for all voltammetric analysis. For example, amperometric current densities of 8.6 A m^{-2} are obtained after 79 h of reactor operation compared to catalytic current densities from CV of only 5.8 A m^{-2}. Recently Katuri *et al.*[14] and Snider *et al.*[16] reported on a simple model (equation 1) of the catalytic CV response at slow scan rates, assuming that the current at each potential in a scan reflects a Nernstian equilibrium distribution of the oxidized and reduced dominant redox species responsible for transferring electrons between the biofilm and the electrode,

$$j = \frac{j_{\lim}}{1 + \exp\left\{\frac{nF(E^{0'} - E)}{RT}\right\}} \qquad (1)$$

where j_{lim} is the limiting current density and $E^{0'}$ categorizes the formal redox potential of the dominant redox species. This approach, as previously demonstrated,[11] permits fitting of the anodic linear sweep voltammogram from CV (Figure 3B), at each biofilm thickness, to the model for n = 1 (Figure 3C dashed line), once a correction for the iR drop between the working and reference electrodes is applied (Figure 3C grey line). In this case CVs recorded for all biofilms provide an estimate of an average 80 Ω iR drop in the electrochemical reactor. This iR drop may be due to electrolyte conductivity, based on the distance between reference and working electrode(s) and the conductance of the electrolyte medium.[14, 16, 39, 40] For example, an estimate of 78 Ω uncompensated resistance is obtained using a conductivity of 1.44 S/m for the electrolyte culture medium,[37] an electrode area of 1.77×10^{-4} m^2 and an approximate distance between working and reference electrodes of 0.020 m.

To attempt to correlate current generation with biofilm thickness, CLSM imaging of sampled working electrodes was used to estimate biofilm thickness as a function of time, as reported on by others.[15, 41] Each sampled graphite rod electrode was cross-sectioned into pieces (2-3 mm) for imaging, Fig. 4A, providing average biofilm thicknesses of 5 ± 2 µm, 17 ± 3 µm and 50 ± 9 µm for the biofilms on the electrodes sampled at 65, 79, and 129 h respectively (see Supplementary Information for additional CLSM images, and z-stack analysis). For comparison, Marsili *et al.*[15] use CLSM to estimate GS biofilm thickness of ~15 µm after 72 h of growth with 20 mM acetate as the electron donor whilst Liu *et al.*[7] estimate formation of 30 µm thick GS biofilms after 96 h of growth with 30 mM acetate as the electron donor, using CLSM. electroactive biofilms. In addition, Laspidou *et al.*[42] report that the outermost layers of heterogeneous biofilms are fluffy, while the surface-associated layers are 5–10 times more dense than the layers near the top of the biofilm.

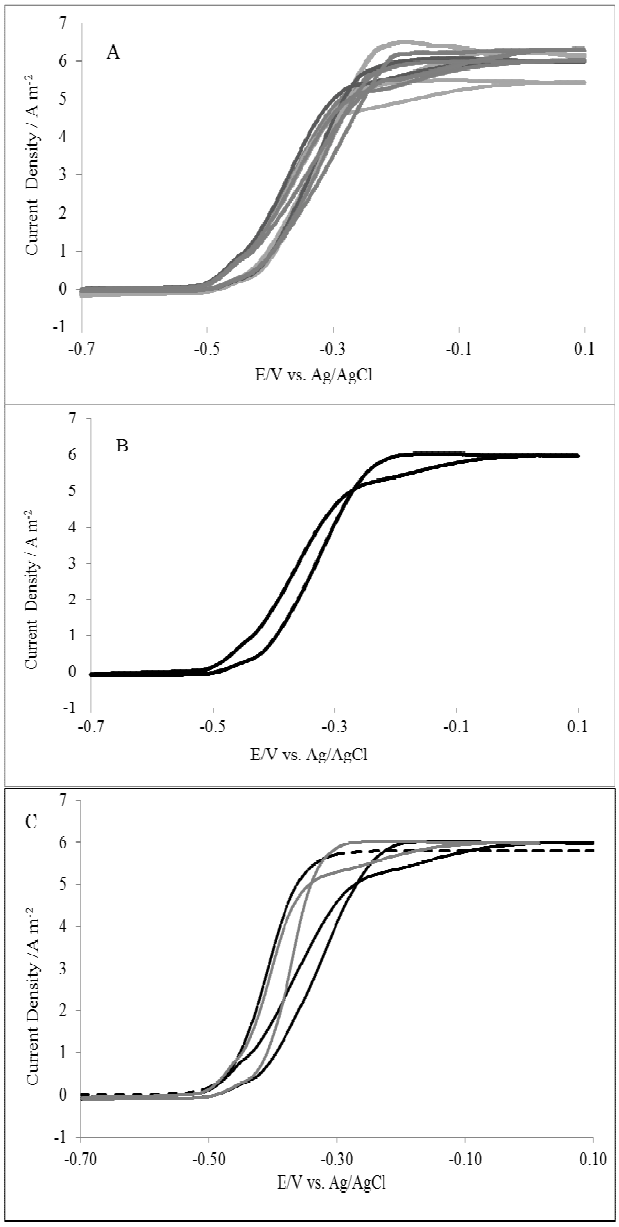

Fig. 3: Cyclic voltammetry (1 mV s^{-1}) at graphite-rod electrodes after 79 h reactor operation recorded for A) each of 6 working electrodes individually, B) all 6 working electrodes simultaneously. C) shows the recorded CV response from B (black) corrected for 80 Ω iR drop (grey), compared to the model of equation 1 with n = 1 (dashed line), with $E^{0\prime}$ = −0.41 V vs. Ag/AgCl and j_{lim} of 5.8 A m^{-2}.

Electron microscopy is used to examine morphological structure, cell attachment, topography and bacterial cell distribution in GS biofilms on the surfaces. The images show formation of a thin layer of bacterial cells on the electrode surface sampled after 65 h Figure 4B, with much thicker biofilms with multiple layers of GS cells apparent for growth over longer time periods, Fig. 4C and 4D, as observed by others[7, 43, 44] The presence of characteristic 2 µm long rod-shaped bacteria in all the SEM images is comparable to the dimensions reported for GS cells, and the images are similar to those observed by others for biofilms grown on graphite electrodes.[8, 28, 37] It should be noted that the biofilms, as

evident from Figure 4, present more complex geometric features (channels, gaps and protrusions) as a function of film thickness, as recently confirmed by Virdis *et al.*[19] using non-invasive confocal Raman microscopy to image ~20 µm thick biofilms grown from wastewater inoculum on graphite rods.

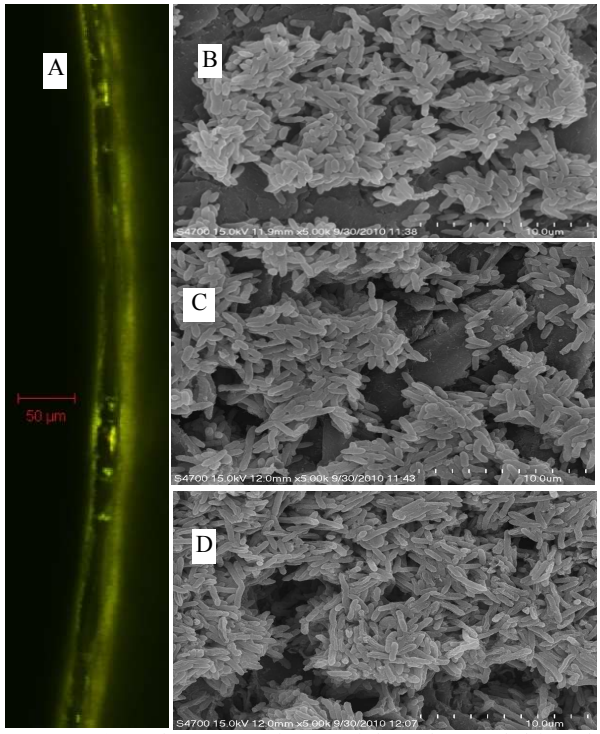

Fig. 4: CLSM (A) and SEM (B-D) images of electrodes sampled from the reactor at 79 h (A, C), 65 h (B), and 129 h (D).

In our reactor a 3.4 fold increment in biofilm thickness (from 5 µm to 17 µm) is observed from 65 h to 79 h of reactor operation, whilst the acetate oxidation current density, based on the amperometric and voltammetric data, results in only an approximately 2 fold increment over the same time period. A further ~3 fold increment in biofilm thickness (from 17 µm to 50 µm) observed from 79 h to 129 h of reactor operation results in only a ~1.2 fold increment in current density over the same time period. This lack of direct correlation between film thickness and catalytic current implies that either mass or charge transport limits the overall catalytic current or that the biofilm formed over time displays differences in bacterial cell densities, viability and/or redox response. In addition, Bond *et al.*[27] report that generation of protons by cells within a GS biofilm anode oxidizing acetate, and their diffusion out of the biofilm, is predicted to result in the formation of a proton concentration gradient across the biofilm. In this gradient, a drop in the pH value is expected to occur close to the biofilm/anode interface. This drop becomes more pronounced as the biofilm grows thicker. The lower pH that this gradient generates at this interface may affect the metabolic activity of the cells in those layers, perhaps contributing to the lack of correlation between acetate oxidation current density and biofilm thickness.

The CV response for biofilms under non-turnover conditions can provide detail on the surface concentration of redox species.[14] Typical non-turnover voltammograms of GS biofilms are shown in Fig. 5 each displaying peaks associated with more than one redox couple (see Supplementary Information for additional scans). For example, the non-turnover response for the biofilm sampled after 65 h (5 µm thickness, Fig. 5A) clearly shows redox transitions, additional to the main transition centered at −0.41 V, centered at −0.6 V and a shoulder on the main redox transition at around −0.48 V for oxidation and −0.37 V for reduction. The peak at −0.6 V is electrocatalytically inactive as no current generation is observed in a medium with substrate at this potential, as reported on recently.[17,13] The non-turnover response for biofilms sampled at later times from the reactor (129 h, 50 µm thickness, Fig. 5B) is also complex, displaying a broad oxidation peak at −0.37 V with a pre-peak shoulder obvious at −0.48 V and numerous un-resolved reduction peaks. *Geobacter sulfurreducens* produces multiple membrane associated cytochromes[8, 45] that can be differentially expressed in the organism during metabolism.[11, 24, 28, 43] The redox potentials of some of these cytochromes have been characterized as −0.370 V vs. AgCl [30,46], −0.300 and −0.390 V vs. AgCl. [47], −0.48 and −0.37 V vs. AgCl,[13] and −0.46 V vs. AgCl[16].

Under non-turnover conditions, integration of the charge (Q) under a slow scan voltammogram can provide an estimation of the surface coverage of redox species ($\Gamma = Q/nFA$ in mol cm^{-2}) for the biofilms. The diffusion layer thickness in a voltammetric experiment depends on the time scale of the experiment, with diffusion layer thicknesses estimated, at the 5 mV s^{-1} scan rate used, as 15, 26 and 79 µm, (*vide infra*) for films of 5, 17 and 50 µm thickness, respectively, indicating that the time-scale at this scan rate is sufficient to permit full electrolysis of redox species within the films. 5. Whilst surface coverage increases as a function of growth time, and biofilm thickness, the increase does not scale linearly with thickness, as expected. A 3.4 fold increment in biofilm thickness (from 5 µm to 17 µm) results in an approximately 7 fold increment in surface coverage whilst a further ~3 fold increment in biofilm thickness (from 17 µm to 50 µm) results in only a ~2 fold increment in surface coverage. This again implies that the biofilm formed over time displays differences in bacterial cell densities, viability and/or redox site concentration and/or connectivity.

At more rapid scan rates, under non-turnover conditions, and assuming that the rate of heterogeneous electron transfer to the biofilm is not limiting and that diffusion is planar, the CV peak current density response can be modelled, as reported on previously,[14] by the Randles−Sevçik equation 2:

$$j = 0.4463 nFC_{redox}\left(\frac{nF}{RT}\right)^{1/2} D^{1/2}\nu^{1/2} \quad (2)$$

where C_{redox} represents the concentration of redox species (mol cm^{-3}) within the film; ν is the scan rate (V s^{-1}); and D is an apparent diffusion coefficient (cm^2 s^{-1}). Thus, a charge transport related parameter ($D^{½}C_{redox}$) can be extracted from the linear portion of a plot of peak current density as a function of the square root of the scan rate for each biofilm, under these semi-infinite diffusion-limited conditions.

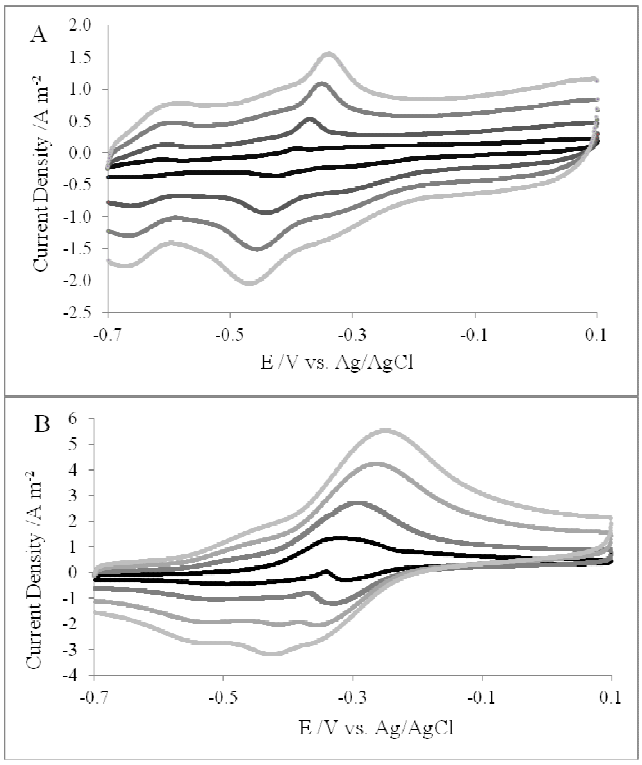

Fig. 5: Cyclic voltammetry recorded at scan rates of 5, 20, 40, 60 mV s^{-1} (from lowest to highest signals) under non-turnover conditions for electrodes sampled from the reactor after A) 65 h and B) 129 h operation.

In the case of redox polymer films on electrodes it has been shown that the diffusion coefficient for electron transport is directly related to the apparent rate of electron exchange[48, 49 50] In films on electrodes, such as those of redox polymers, where physical diffusion of redox species is restricted, charge transport is postulated to arise from electron hopping between adjacent electroactive moieties. The rate of charge, or the charge transport diffusion co-efficient, may thus be limited by electron hopping, ion transport process accompanying the electron hopping to maintain electro-neutrality, or the associated diffusional physical motions of the polymers to bring electron transfer sites into close enough proximity to transfer electrons.[51-53]

A charge transport related parameter ($D^{½}C_{redox}$) of 1.3 ± 0.3 × 10^{-9} mol cm^2 $s^{-1/2}$, 4.8 ± 0.9 × 10^{-9} mol cm^2 $s^{-1/2}$ and 7.5 ± 0.5 × 10^{-9} mol cm^2 $s^{-1/2}$ is obtained for biofilm thicknesses of 5 ± 2, 17 ± 3 and 50 ± 9 µm, respectively. Interestingly, reported $D^{1/2}C_{redox}$ values of 7.2 × 10^{-9} mol cm^2 $s^{-1/2}$ for films of a ferrocene redox polymer[54] and 1.2 × 10^{-8} mol cm^2 $s^{-1/2}$ for films of osmium-based redox polymers[55] on electrodes are comparable to the values obtained for $D^{1/2}C_{redox}$ of GS biofilms in this study, perhaps indicative of a similar mechanism operating for electron transfer through the electroactive biofilms. The surface coverage divided by the average biofilm thickness gives an estimate of the concentration of redox species in the biofilm, C_{redox} of 2.8 ± 1.1, 5.9 ± 1.2 and 4.0 ± 1.1 mM for biofilms of thickness of 5 ± 2, 17 ± 3 and 50 ± 9 µm, respectively, permitting extraction of a value for D from the $D^{½}C_{redox}$ charge transport related parameter. The redox site concentrations estimated are similar to a value of 7.3 mM reported on previously[14] for GS biofilms of 34 µm in thickness induced to grow through successive batch-feed cycles on graphite electrodes.

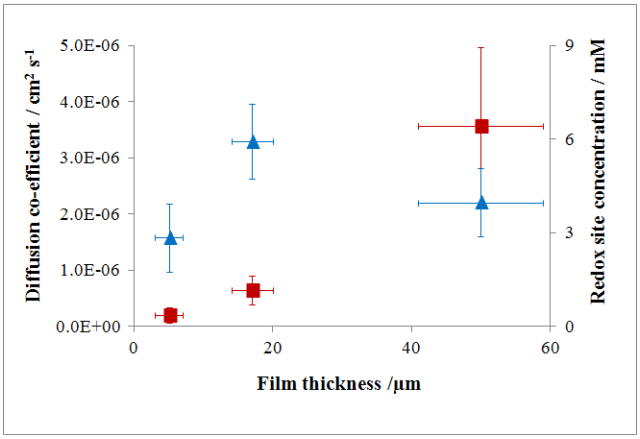

Fig. 6: Plot of D (squares) and of C_{redox} (triangles) versus biofilm thickness.

Diffusion coefficients of 2.1 ± 1.4 × 10^{-7} cm^2 s^{-1}, 6.5 ± 2.5 × 10^{-7} cm^2 s^{-1} and 3.6 ± 1.4 × 10^{-6} cm^2 s^{-1} are thus obtained for biofilm thicknesses of 5 ± 2, 17 ± 3 and 50 ± 9 µm, respectively. These values are, again, similar to a value of 3.6 × 10^{-6} cm^2 s^{-1} reported on previously[14] for GS biofilms of 34 µm in thickness induced to grow through successive batch-feed cycles on graphite electrodes. Diffusion coefficient and redox species concentration are both higher in biofilms of 17 µm thickness over their values in biofilms of 5 µm thickness (Fig. 6). This increase in C_{redox} may be due to a decrease in film porosity, averaged over the entire biofilm, as a function of time, supported by the observation that the surface coverage increases 7-fold whilst film thickness only increases 3.4 fold, when comparing the 17 µm thick biofilm to the 5 µm thick biofilm. The more compact 17 µm thick biofilm has therefore a higher redox site concentration, and more rapid charge transport rate, possibly as a result of closer proximity of redox sites to each other facilitating electron hopping. The redox site concentration in the 50 µm thick biofilm is lower than that estimated in the 17 µm thick biofilm, again possibly because of increased porosity of the outermost layers of the 50 µm thick biofilm, and thus an overall decrease in biofilm GS cell and redox site density. Interestingly a marked increase in D is obtained for charge transport through the 50 µm thick biofilm over that obtained in the thinner films. This can be a result of increased porosity of the thicker films contributing to ease of ion transport through the film, where ion transport may be the limiting factor for charge transport under this condition. Recently Renslow *et al.*[21] reported a bulk liquid water diffusion coefficient value of 2.8 × 10^{-5} cm^2 s^{-1} within GS biofilms with an observation that the diffusion coefficient value for water is lower in the layers close to electrode compared to that in the outermost layers of the biofilms. This solvent transport diffusion coefficient, during acetate oxidation by GS biofilms, is an order of magnitude higher than the highest charge transport diffusion coefficient estimated, again indicative that charge transport may be limited by ion transport, and/or bacterial motions, to affect electron transfer through the films at the latter stage of biofilm growth, and not solvent or electron transfer.

Conclusions

Current generation, as a result of acetate oxidation, reaches a steady-state of 9 A m^{-2} for biofilms of GS induced to grow on graphite electrode under continuous flow conditions in a single-compartment three electrode cell, with 0 V vs Ag/AgCl applied anode potential. The increase in current over time does not scale linearly with film thickness or redox site coverage presumably because either mass or charge transport limits the current or that the biofilm formed over time displays differences in bacterial cell densities, viability and/or redox response. A combination of electrochemical and microscopic studies reveal that the biofilm developed to 50 ± 9 μm thickness after 129 hours, when the catalytic current is at steady-state, displays more rapid charge transport diffusion, even though the overall redox site concentration is lower than in thinner films. Whilst the microbial biofilms may not display homogeneous distribution of cells, or indeed diffusion coefficient[21] across the entire film thickness an increase in the overall biofilm porosity for the 50 μm thick film may contribute to improved charge transport, as ion transport required to maintain electroneutrality within the bulk film upon oxidation may be the limiting factor for charge transport under the non-turnover condition of the experiment. Whether this is also the case when the biofilm oxidising acetate substrate is not clear as yet.

Acknowledgements

Support for this research was provided by a Charles Parsons Energy Research Award through Science Foundation Ireland and an EU FP 7 Marie Curie Intra European Fellowship to AK for Career Development (Grant A/6342-PIEF-GA-2009-237181).

Notes and references

[a] School of Chemistry & Ryan Institute, National University of Ireland Galway, University Road, Galway, Ireland.

[b] Water Desalination and Reuse Research Center, King Abdullah University of Science and Technology, Thuwal, Kingdom of Saudi Arabia.

[c] Present address: Department of Chemical Engineering, Massachusetts Institute of Technology, Cambridge, USA.

1. K. Rabaey and W. Verstraete, *Trends in Biotechnology*, 2005, **23**, 291-298.
2. B. E. Logan, B. Hamelers, R. Rozendal, U. Schröder, J. Keller, S. Freguia, P. Aelterman, W. Verstraete and K. Rabaey, *Environmental Science and Technology*, 2006, **40**, 5181-5192.
3. D. R. Lovley, *Nature Reviews. Microbiology*, 2006, **4**, 497-508.
4. O. Schaetzle, F. Barrière and K. Baronian, *Energy and Environmental Science*, 2008, **1**, 607-620.
5. D. Baron, E. LaBelle, D. Coursolle, J. A. Gralnick and D. R. Bond, *Journal of Biological Chemistry*, 2009, **284**, 28865-28873.
6. K. P. Nevin, B. C. Kim, R. H. Glaven, J. P. Johnson, T. L. Woodward, B. A. Methé, R. J. Didonato Jr, S. F. Covalla, A. E. Franks, A. Liu and D. R. Lovley, *PLoS ONE*, 2009, **4**.
7. Y. Liu, H. Kim, R. R. Franklin and D. R. Bond, *ChemPhysChem*, 2011, **12**, 2235-2241.
8. S. M. Strycharz-Glaven, R. M. Snider, A. Guiseppi-Elie and L. M. Tender, *Energy & Environmental Science*, 2011, **4**, 4366-4379.
9. N. S. Malvankar, M. Vargas, K. P. Nevin, A. E. Franks, C. Leang, B.-C. Kim, K. Inoue, T. Mester, S. F. Covalla, J. P. Johnson, V. M. Rotello, M. T. Tuominen and D. R. Lovley, *Nature Nanotechnology*, 2011, **6**, 573-579.
10. D. R. Bond, D. E. Holmes, L. M. Tender and D. R. Lovley, *Science*, 2002, **295**, 483-485.
11. H. Richter, K. P. Nevin, H. Jia, D. A. Lowy, D. R. Lovley and L. M. Tender, *Energy and Environmental Science*, 2009, **2**, 506-516.
12. N. S. Malvankar, M. T. Tuominen and D. R. Lovley, *Energy and Environmental Science*, 2012, **5**, 5790-5797.
13. X. Zhu, M. D. Yates and B. E. Logan, *Electrochemistry Communications*, 2012, **22**, 116-119.
14. K. P. Katuri, S. Rengaraj, P. Kavanagh, V. O'Flaherty and D. Leech, *Langmuir*, 2012, **28**, 7904-7913.
15. E. Marsili, J. B. Rollefson, D. B. Baron, R. M. Hozalski and D. R. Bond, *Applied and Environmental Microbiology*, 2008, **74**, 7329-7337.
16. R. M. Snider, S. M. Strycharz-Glaven, S. D. Tsoi, J. S. Erickson and L. M. Tender, *Proceedings of the National Academy of Sciences*, 2012, **109**, 15467-15472.
17. K. Fricke, F. Harnisch and U. Schröder, *Energy and Environmental Science*, 2008, **1**, 144-147.
18. D. Millo, F. Harnisch, S. A. Patil, H. K. Ly, U. Schröder and P. Hildebrandt, *Angewandte Chemie International Edition*, 2011, **50**, 2625-2627.
19. B. Virdis, F. Harnisch, D. J. Batstone, K. Rabaey and B. C. Donose, *Energy & Environmental Science*, 2012, **5**, 7017-7024.
20. C. Leang, X. Qian, T. Mester and D. R. Lovley, *Applied and Environmental Microbiology*, 2010, **76**, 4080-4084.
21. R. S. Renslow, J. T. Babauta, P. D. Majors and H. Beyenal, *Energy & Environmental Science*, 2013, **6**, 595-607.
22. E. Marsili, J. Sun and D. R. Bond, *Electroanalysis*, 2010, **22**, 865-874.
23. S. M. Strycharz, A. P. Malanoski, R. M. Snider, H. Yi, D. R. Lovley and L. M. Tender, *Energy & Environmental Science*, 2011, **4**, 896-913.
24. D. E. Holmes, S. K. Chaudhuri, K. P. Nevin, T. Mehta, B. A. Methé, A. Liu, J. E. Ward, T. L. Woodard, J. Webster and D. R. Lovley, *Environmental Microbiology*, 2006, **8**, 1805-1815.
25. K. Inoue, X. Qian, L. Morgado, B. C. Kim, T. Mester, M. Izallalen, C. A. Salgueiro and D. R. Lovley, *Applied and Environmental Microbiology*, 2010, **76**, 3999-4007.
26. B. C. Kim, B. L. Postier, R. J. DiDonato, S. K. Chaudhuri, K. P. Nevin and D. R. Lovley, *Bioelectrochemistry*, 2008, **73**, 70-75.
27. D. R. Bond, S. M. Strycharz-Glaven, L. M. Tender and C. I. Torres, *ChemSusChem*, 2012, **5**, 1099-1105.
28. D. R. Bond and D. R. Lovley, *Applied and Environmental Microbiology*, 2003, **69**, 1548-1555.
29. J. Kuo, *Electron Microscopy: Methods and Protocols*, Humana Press, 2007.
30. S. Seeliger, R. Cord-Ruwisch and B. Schink, *Journal of Bacteriology*, 1998, **180**, 3686-3691.
31. A. Kumar, A. Siggins, K. Katuri, T. Mahony, V. O'Flaherty, P. Lens and D. Leech, *Chemical Engineering Journal*, 2013, **230**, 532-536.
32. H.-S. Lee, C. s. I. Torres, P. Parameswaran and B. E. Rittmann, *Environmental science & technology*, 2009, **43**, 7971-7976.
33. A. Kumar, K. Katuri, P. Lens and D. Leech, *Biochemical Society Transactions*, 2012, **40**, 1308-1314.
34. K. P. Katuri, P. Kavanagh, S. Rengaraj and D. Leech, *Chemical Communications*, 2010, **46**, 4758-4760.
35. J. Babauta, R. Renslow, Z. Lewandowski and H. Beyenal, *Biofouling*, 2012, **28**, 789-812.
36. S. M. Strycharz, R. H. Glaven, M. V. Coppi, S. M. Gannon, L. A. Perpetua, A. Liu, K. P. Nevin and D. R. Lovley, *Bioelectrochemistry*, 2011, **80**, 142-150.
37. C. I. Torres, A. K. Marcus, P. Parameswaran and B. E. Rittmann, *Environmental Science and Technology*, 2008, **42**, 6593-6597.
38. S. Srikanth, E. Marsili, M. C. Flickinger and D. R. Bond, *Biotechnology and Bioengineering*, 2008, **99**, 1065-1073.

39. C. I. Torres, A. K. Marcus, H. S. Lee, P. Parameswaran, R. Krajmalnik-Brown and B. E. Rittmann, *FEMS Microbiology Reviews*, 2010, **34**, 3-17.
40. H. Yi, K. P. Nevin, B. C. Kim, A. E. Franks, A. Klimes, L. M. Tender and D. R. Lovley, *Biosensors and Bioelectronics*, 2009, **24**, 3498-3503.
41. K. P. Nevin, H. Richter, S. F. Covalla, J. P. Johnson, T. L. Woodard, A. L. Orloff, H. Jia, M. Zhang and D. R. Lovley, *Environmental Microbiology*, 2008, **10**, 2505-2514.
42. C. S. Laspidou and B. E. Rittmann, *Water Research*, 2004, **38**, 3362-3372.
43. G. Reguera, K. P. Nevin, J. S. Nicoll, S. F. Covalla, T. L. Woodard and D. R. Lovley, *Applied and Environmental Microbiology*, 2006, **72**, 7345-7348.
44. H. Richter, K. McCarthy, K. P. Nevin, J. P. Johnson, V. M. Rotello and D. R. Lovley, *Langmuir*, 2008, **24**, 4376-4379.
45. B. A. Methé, K. E. Nelson, J. A. Eisen, I. T. Paulsen, W. Nelson, J. F. Heidelberg, D. Wu, M. Wu, N. Ward, M. J. Beanan, R. J. Dodson, R. Madupu, L. M. Brinkac, S. C. Daugherty, R. T. DeBoy, A. S. Durkin, M. Gwinn, J. F. Kolonay, S. A. Sullivan, D. H. Haft, J. Selengut, T. M. Davidsen, N. Zafar, O. White, B. Tran, C. Romero, H. A. Forberger, J. Weidman, H. Khouri, T. V. Feldblyum, T. R. Utterback, S. E. Van Aken, D. R. Lovley and C. M. Fraser, *Science*, 2003, **302**, 1967-1969.
46. J. R. Lloyd, A. L. H. Myerson, C. Leang, M. V. Coppi, S. Cuifo, B. A. Methè, D. Lovley and S. J. Sandler, *Biochem J*, 2003, **369**, 153-161.
47. T. S. Magnuson, A. L. Hodges-Myerson and D. R. Lovley, *FEMS Microbiology Letters*, 2000, **185**, 205-211.
48. H. Dahms, *The Journal of Physical Chemistry*, 1968, **72**, 362-364.
49. I. Ruff, V. J. Friedrich, K. Demeter and K. Csillag, American Chemical Society, 1971.
50. I. Ruff, *The Journal of Physical Chemistry*, 1965, **69**, 3183-3186.
51. P. Kavanagh and D. Leech, *Physical Chemistry Chemical Physics*, 2013, **15**, 4859-4869.
52. F. Mao, N. Mano and A. Heller, *Journal of the American Chemical Society*, 2003, **125**, 4951-4957.
53. D. N. Blauch and J. M. Saveant, *The Journal of Physical Chemistry*, 1993, **97**, 6444-6448.
54. C. Bunte, O. Prucker, T. König and J. r. Rühe, *Langmuir*, 2009, **26**, 6019-6027.
55. D. Macaodha, M. L. Ferrer, P. O. Conghaile, P. Kavanagh and D. Leech, *Phys Chem Chem Phys*, 2012, **14**, 14667-14672.